RESEARCH | Article in Press

Determination of neutron radiation fields and exposure in geological repositories for high-level spent-fuel radioactive waste

Sushanta Biswas · Frank B. E. Becker · Ron Dagan

Received: 16 February 2026 / Accepted: 2 September 2026

Abstract
The proper and safe disposal of heat-generating nuclear waste from commercial nuclear power plants is the subject of social controversy. This work focuses on the German concept of final storage in rock salt, which is considered a reference for the option of deep geological final storage. Due to the current search campaign for a final storage site in Germany, which also includes the options of final storage in clay formations and granite, these options were also investigated. Monte Carlo simulations were performed to obtain information about the radiation field and the associated dosimetry. Past studies have shown that direct neutron irradiation, together with neutrons backscattered in the emplacement drift, represent the most significant contribution to the external irradiation of workers. A model of a shielding cask was employed for the simulations and a representative waste inventory was used, based on the estimated total amount of spent fuel elements available in Germany. The neutron radiation field was investigated with regard to the surrounding host rock layers and concrete lining. Location depending exposure to workers in the vicinity of storage casks in horizontal emplacement drifts were investigated with and without a drift branch. As a result, the dose rate is significantly higher in some locations at a 90° branch compared to a straight drift due to the scattering in this area. The position-dependent influence of PET absorber rods in the cask is briefly outlined. The implementation of an improved neutron scattering formalism (DBRC) showed a small but noticeable reduction in dose rate.

Highlights

- Investigation of neutron-induced ambient dose rates in emplacement drifts with branches using the Monte Carlo method.
- Improved neutron scattering formalism (DBRC).

Keywords Deep geological repository · High-level nuclear waste · Radiation field · Neutron ambient dose rate · Doppler broadening rejection correction (DBRC) · Monte Carlo code MCNP

https://doi.org/10.1007/s42452-026-09516-x

Published online: 11 September 2026

1 Introduction

In the context of the ongoing search for a deep geological disposal site for high-level radioactive waste in Germany, three types of host rock are currently being considered: clay, rock salt, and crystalline rock. As a result of the handling of the waste during storage and the retrieval option, the issue of occupational radiation exposure in the storage drift must be taken into account. In particular, it was shown that neutrons are the dominant contributors to the dose and are of great importance due to their high backscattering in the drift (see [13]). This article therefore evaluates the radiation field in salt- and concrete-lined final storage drifts with a particular focus on neutron scattering. To obtain information about the radiation field and the associated dosimetry information, Monte Carlo simulations with the Code MCNP6.2 [16] were performed, whereby the double differential scattering cross section for the backscattering of neutrons in the storage drifts is decisive. A simplified model of a shielding container was used for the simulations, and a representative waste inventory was determined based on the estimated total amount of spent fuel elements available in Germany [11]. The neutron radiation field was investigated with regard to the surrounding host rock layers and concrete lining. Neutron ambient dose rates in the vicinity of shielding containers located in a horizontal storage drift were investigated. This, first of its kind contribution, as far as the scattering kernel is concerned, for future postulated design of radioactive disposal focuses thereafter extensively on the improved accurate available interaction description of neutrons with the walls of the different repository types and gallery geometries. The implementation of an improved neutron scattering formalism confirms that, in the case under study, the approximated solution was good enough. Nevertheless, it is obviously recommended to use a physical realistic, improved model, as its availability was proved in this study.

2 Methods and methodology

2.1 Spent nuclear fuel as a neutron source

Management of spent nuclear fuel (SNF) is difficult due to its intense radioactivity, heat generation, the half-lives of the isotopes, and its migration characteristic. Consequently, SNF is kept first in an interim storage to allow for thermal cooling and radioactive decay before final disposal. This step allows for a decay of isotopes with very short half-lives and reduces considerably the radiotoxicity of the SNF. Under the multi-barrier concept, waste is eventually placed in deep geological repositories within specialized storage casks. The shielding of these casks is a strategic compromise, balancing the mass required for handling against the imperative to minimize radiation dose.

Based on the average inventory of spent fuel elements from pressurized water reactors (PWR) in Germany [11], a representative waste load of 90% uranium oxide (UOX) fuel and 10% mixed oxide (MOX) fuel with an average burnup of 55 GWd/t(HM) was assumed. In order to take into account an interim storage period, the user-friendly online program Nucleonica [9], which is based on the improved burnup code KORIGEN, was used to calculate the remaining activity of the spent fuel inventory after 50 years.

From previous investigations, it is known that neutrons dominate the radiation field and exposure outside the shielding cask [10]. The contribution of backscattered neutrons of the host rock layers or the concrete lining plays an important role [13].

Consequently, only those isotopes that make a significant contribution to neutron activity were considered in this work. The neutron production rates and spectra were determined using the SOURCES code [17], taking into account neutrons from spontaneous fission, (α, n) reactions, and delayed neutron emission. The neutron source strength was calculated to be 2.13×10^9 neutrons/s for the total spent fuel inventory of a single cask. Table 1 lists the dominant neutron emitters that were found from the above calculation [14].

Table 1 Parameters in neutron source term specification (Saurí Suárez et al., 2018)

Parameter	Description/ Value
Inventory	90% UOX fuel and 10% MOX fuel
Average burnup	55 GWd/t(HM)
Spent fuel age	50 years
Neutron emitters (spontaneous fission)	^{244}Cm (93%), ^{246}Cm (5%), ^{238}Pu, ^{240}Pu, ^{242}Pu combined (~2%)
Neutron source strength	2.13×10^9 neutrons/s

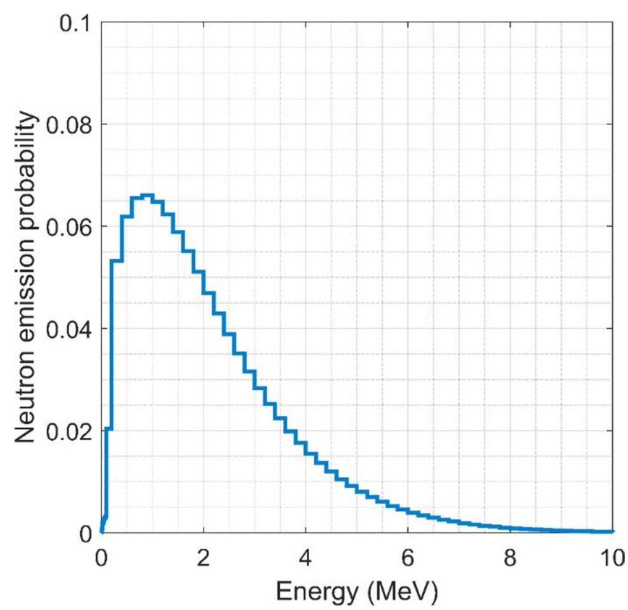

Fig. 1 Normalized neutron energy spectrum of the spent fuel inventory of a single cask (The parameters in neutron source term specification and the normalized neutron energy spectrum of the spent fuel inventory of a single cask were taken from Saurí Suárez et al. (2018))

A neutron energy spectrum was generated to define a neutron source representative of the spent fuel elements (see Fig. 1). This spectrum represents the effective spent fuel inventory and was used as the basis for the following simulations.

2.2 Monte Carlo simulations

The Monte Carlo code MCNP® version 6.2 [16] was used to calculate the radiation field around a POLLUX®-10 type shielding cask [5, 8] loaded with spent fuel elements. Detailed dimensions and technical drawings can be found in [4, 8]. The neutron source properties mentioned above were used to insert a representative volume source into the POLLUX®-10 cask. Overall, the following assumptions and simplifications were made for the simulations (see Fig. 2): For the structure of the POLLUX®-10 cask model in MCNP®, a symmetrical cask design was chosen for simplification purpose. It was assumed that spent fuel elements inside the cask were distributed homogeneously in a cylindrical geometry within the active zone. The inactive zones at the upper and lower ends of the spent fuel elements were modeled as consisting of zircaloy.

The shielding components of the cask consist of an inner shield made of stainless steel and an outer shield made of cast iron. Two rings made of polyethylene (PET) rods are embedded in the outer shield. Each layer consists of 36 PET rods, each with a radius of 3.75 cm. 10 cm thick graphite plates are attached to the upper and lower parts of the cask housing. Homogeneous spent fuel elements are placed in a cylinder with a diameter of 69 cm in the center of the inner shield. The total length of the cask amounts to 5.51 m with a diameter of 1.56 m. The employed MCNP® model is shown in Fig. 2. A cask is located 2.63 m from the end wall of the gallery in the center of the drift. The drift geometries were based on the generic deep repository models of Stahlmann et al. [15], according to the German mining standard, and are constructed with curved surfaces with a maximum

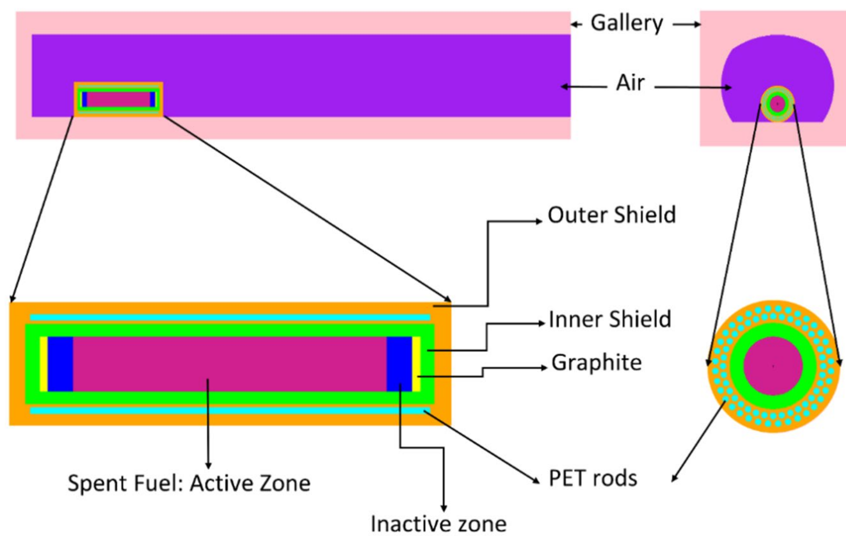

Fig. 2 Schematic drawing of a cask placed in a horizontal storage gallery. This simplified representation based on the simulation model is not to scale and is therefore for illustrative purposes only

height of 3.7 m and a maximum horizontal extension of at least 20 m. The material of the gallery walls was either concrete or rock salt with a thickness of 1.5 m. Storage scenarios were investigated in which casks were placed horizontally in an emplacement drift according to the proven storage concept in rock salt [4, 5].

The MCNP® simulations were carried out in two steps. First based on the neutron energy spectrum described in Sect. 2.1, the emitted neutrons from outer surfaces of the POLLUX®-10 cask free in air were calculated using the Surface Source Write (SSW) feature in MCNP®. In this step, the neutron interactions (e.g., fission, (n, xn) reactions) within the cask were accounted for and the particle history and tracks of the neutrons escaped through the outer surface were recorded as a surface neutron source. On the second step, the recorded surface neutron source was reused in subsequent simulations to calculate the dose rates and neutron flux in different gallery conditions. On the other hand, the transport of re-entered neutrons to the cask were explicitly calculated based on the material composition within the cask. This two-step approach allowed shorter calculation time while maintaining a high accuracy and relevant physics. Separate surface sources were created to account for the changes in cask geometry (e.g. PET configurations). Point detector arrays (F5) were used to obtain the neutron fluxes at various locations in the drifts. In turn, ambient dose equivalent rates were calculated from the detector fluxes employing fluence to dose conversion factor from ICRP Publication 74, Annals of the ICRP (ICRP, [6]).

2.3 Impact of PET rods

High-energy neutrons are slowed down by interacting with the two rings of PET rods in the outer shielding of the POLLUX®-10 container and can then be absorbed in the shielding material (see Fig. 2). To illustrate the effect of the PET rods, the neutron flux was calculated in four different configurations: without PET rods, with only the inner or outer ring, and with both rings. Neutron spectra emitted at the surface of the cask in such configurations were calculated and reported hereafter.

2.4 MCNP® and the improved neutron scattering formalism DBRC

Two different simulations were performed for the same scenarios, both using the “Doppler Broadening Resonance Correction (DBRC)” method and the standard MCNP® option. DBRC refers to the implementation of an improved neutron scattering formalism that considers more accurate elastic neutron scattering based on the resonant structures. Consequently, the two main former approximations (zero degree and constant cross section)

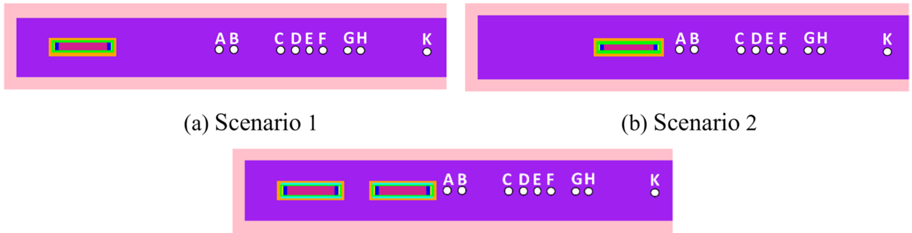

(a) Scenario 1 (b) Scenario 2

(c) Scenario 3

Fig. 3 Schematic representation of the investigated straight galleries. Top view in relation to Fig. 2. Scenario 1: Single cask far inside the gallery; Scenario 2: Single cask closer to the middle of the gallery; Scenario 3: Two casks placed 2.0 m apart from each other. The point detectors are placed at nine different positions (designated by **A**, **B**, **C**…). (c) Scenario 3

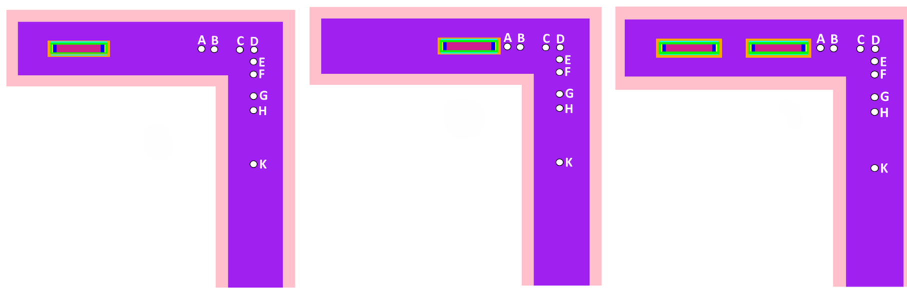

(a) Scenario 4 (b) Scenario 5 (c) Scenario 6

Fig. 4 The three scenarios examined for a gallery branch with a right-angled geometry (top view). Scenario 1: Single cask far from the bending; Scenario 2: Single cask closer to the bending; Scenario 3: Two casks placed 2.0 m apart from each other. The detectors are placed at nine different positions (designated by **A**, **B**, **C**…)

are released. Therefore, the elastic neutron scattering in particular in the lower keV range is physically accurate. A complete description of the double differential, resonance, and temperature-dependent scattering kernel was developed by Rothenstein and Dagan [12], and the treatment of resonance scattering was implemented in Monte Carlo codes by Becker [1]. In the new version of MCNP® Version 6.3 this model is now also available. The 6.3 version of the code was not available to the authors.

This study used a modified version of MCNP® Version 6.2, with the DBRC mechanism set for incident neutrons with an energy of less than 50 keV. For the simulations with the above simplifications, a temperature of 600 K was assumed for the spent fuel elements, while all other materials, including shielding and tunnel walls, were considered at a temperature of 300 K. The DBRC method was applied to all materials, including spent fuel elements, shielding, and emplacement drift walls, for incident neutrons with energies below 50 keV. With MCNP® the ambient dose equivalent rate for neutrons at different point detector locations were calculated in a salt and concrete gallery at various points with and without the DBRC option. MCNP® output values are reported along with the estimated relative error. The number of simulated source particles amounted to 5×10^8 in order to achieve acceptable statistical errors; a value of approximately 1% or less was employed for the estimated relative error as the selection criterion. For further details, see [2].

2.5 Storage scenarios and emplacement drift geometries

Representative storage scenarios were investigated in which casks were placed horizontally in a drift. Two different emplacement drift geometries were investigated: simulations were carried out for a straight drift and a drift with a right-angled geometry. Figures 3 and 4 illustrate the employed arrangement of casks in these emplacement drifts.

The following scenarios were selected, with the casks placed along the symmetry axis of the drift. For straight galleries: scenario 1 with one cask at the far end of the gallery 2.63 m away from the end wall, scenario 2 with a container placed in the middle of the tunnel, 10.41 m away from the end wall, and scenario 3: combining

 https://doi.org/10.1007/s42452-026-09516-x

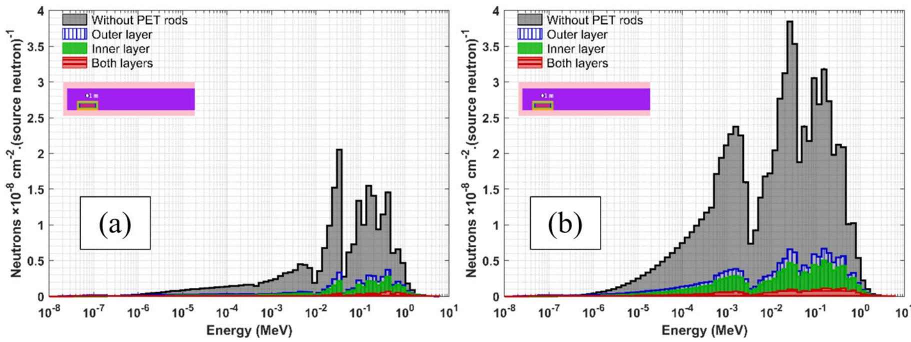

Fig. 5 Neutron flux spectra for four different PET rod scenarios for free in air (**a**) and salt gallery (**b**)

Table 2 Importance of different PET rod configurations on the total neutron flux in free in air and in a salt gallery

PET rods configuration	Total neutron flux (neutron.cm^{-2}. (source neutron)$^{-1}$	
	Free in air	In salt gallery
Without PET rods	$2.43\times10^{-7}\pm0.05\%$	$7.53\times10^{-7}\pm0.04\%$
Outer layer	$4.87\times10^{-8}\pm0.12\%$	$1.46\times10^{-7}\pm0.08\%$
Inner layer	$3.32\times10^{-8}\pm0.15\%$	$1.06\times10^{-7}\pm0.09\%$
Both layers	$7.91\times10^{-9}\pm0.19\%$	$2.54\times10^{-8}\pm0.14\%$

scenarios 1 and 2 with two casks spaced 2 m apart. For the dose calculations with MCNP®, point detectors (F5-Tally) were placed at the various positions A to K. Similarly, scenarios 3–6 shown in Fig. 4 were chosen for a right-angled drift arrangement.

3 Results and discussion

3.1 Impact of PET rods on the radiation field in a drift

The outer shielding of the POLLUX®-10 container consists of two rings made of PET rods (see Fig. 2). Interaction with these rings allows the neutrons to be moderated and then absorbed by the shielding material. As mentioned in Sect. 2.3, the neutron flux was calculated for four different configurations: without PET rods, with only the inner or outer ring, and with both rings. Figure 5 shows the results regarding their effect on the neutron flux spectrum at a point detector placed 1 m to the side of the cask. The shown scenarios are free in air and in a salt emplacement drift. Comparison of total neutron flux between different configurations of PET rods are presented in Table 2.

As seen in Table 2, the total flux in the salt gallery is for all cases about three times higher than free in air. This result emphasizes the backscattering of the materials of gallery walls. In the salt gallery in particular, backscattering from chlorine nuclei is about five times higher than from sodium nuclei. Here it should be mentioned that the standard scattering procedure is approximated at 0 °K. This assumption is analyzed in this study with an improved scattering model, as discussed in Sect. 2.4.

Without PET rods, the total neutron flux amounts to 2.43×10^{-7} cm^{-2} neutrons per source neutron in free in air, whilst the neutron flux in the salt gallery is about three times higher, at 7.53×10^{-7} cm^{-2} neutrons per source neutron. The importance of the PET rods to reduce the neutron flux is pronounced in Table 2. With two PET rings, the total neutron flux is reduced by a factor of about 30 for free in air and salt gallery. Inserting only the inner layer has a slightly lower shielding effect than the outer layer. For example, for the scenario free in air with only the inner or outer ring, a total neutron flux of 3.32×10^{-8} cm^{-2} or 4.87×10^{-8} cm^{-2} was calculated, respectively. It points out that neutron moderation and absorption depend not only on the number of PET rods employed, but also on their position within the cask. As the number of rods is the same in the inner and outer layer of the

POLLUX®-10 cask due to stability and construction considerations, the spacing between the PET rods in the outer layer is larger and hence allows for less moderation and absorption. Consequently, the configuration with an outer layer exhibits higher neutron-flux values. This emphasizes the importance of finding a balance between the material properties and design consideration of the POLLUX®-10 cask in view of the neutron flux around.

3.2 Impact of host rock on the radiation field

Since scattered neutrons play a significant role for the radiation field in a gallery, the question arises as to the impact of host rock on the radiation field and dose. First, the spectra of the neutron fluxes were determined considering both layers of PET rods based on the lowest flux shown in the former section. Radiation fields were calculated for the three scenarios: free in air, salt, and concrete.

As shown in Fig. 6, the flux was determined in the straight emplacement drift in Fig. 3 at the point detector positions 0.5 m, 1 m, 5 m, and 10 m away from the cask along its axis of symmetry. For casks placed in the salt gallery or in galleries with concrete lining, an increase in the neutron flux can be observed compared to those free in air, particularly for the rock salt scenario in the energy range of 0.02 to 1 MeV. This increase is even more pronounced at greater distances from the cask. The scenario drift with concrete lining shows a less pronounced increase compared to rock salt.

In addition, the concrete scenario shows a significant number of thermal neutrons in the range of 0.025×10^{-6} MeV, see Table 3, and a reduced amount of high energy neutrons. This can be explained by the presence of lighter isotopes such as 1 wt% hydrogen and 50 wt% oxygen in concrete which effectively thermalized more neutrons. According to Table B.3 in ICRP Publication 103, Annals of the ICRP (ICRP, [7]), the radiation weighting factor for neutron energies below 10 keV is 5, while it is 20 in the energy range from 100 keV to 2 MeV. As a result, the dose attributed to the neutron flux in the concrete gallery is lower than for rock salt.

3.3 Impact of emplacement drift geometry

Based on the scenarios shown in Figs. 3 and 4, dose rates for different geometries are presented for the emplacement drift with wall materials salt and concrete. Three different emplacement scenarios are considered: one cask placed 2.63 m away from the end wall of the gallery (scenarios 1 and 4), one cask placed 2 m away from this position (scenarios 2 and 5), and both casks together at the aforementioned positions (scenarios 3 and 6).

The results shown in Fig. 7 indicate that higher dose rates occur in scenarios 2 and 3, as the distance between the detectors and the cask is shorter in scenarios 2 and 3. For scenario 2, with the straight emplacement gallery in salt, the neutron dose rate at point A, which is 1.0 m away from the cask, amounts to 7.0 μSv/h. In comparison, the value in scenario 1, is only 0.6 μSv/h, as the detector A is located 8.5 m away from the cask. In scenario 3, both casks are placed in the drift. The neutron dose rate is then 7.2 μSv/h, but remains lower than the sum of the dose rates of scenarios 1 and 2, because the second container shields the first. A cask acts as a physical absorption barrier, preventing neutrons from the shielded cask from reaching the detector. This geometric shadowing significantly reduces the secondary contribution of scattered neutrons from the gallery walls. The same applies to scenarios 4 to 6 in the storage scenario with the 90° branch. Comparing the gallery with the 90° branch with the straight gallery, the values for positions A to D are observed to be similar. This indicates that, due to the identical geometry in this area, no significant influence of the changed geometry of the subsequent branch is apparent.

The influence of the branch becomes noticeable when one compares the detectors D to G. In case of rock salt, for the straight gallery the neutron dose rates at points E and F amount to: 0.22 and 0.18 μSv/h for scenario 1, 1.01 and 0.80 μSv/h for scenario 2, 1.14 and 0.90 μSv/h for scenario 3, respectively.

In the gallery with the 90° branch, the observed dose rates for points E and F are: 0.26 and 0.24 μSv/h for scenario 4, 1.23 and 1.10 μSv/h for scenario 5, and 1.52 and 1.42 μSv/h for scenario 6, respectively.

For point detector E, the values are approximately 18, 22, and 33% higher for the branch case. The dose within the branch case is even more pronounced for the point detector F, with higher values of 33, 38, and 58%.

Fig. 6 Distance dependent neutron flux spectra for the three scenarios free in air (**a**), salt gallery (**b**) and drift with concrete lining (**c**)

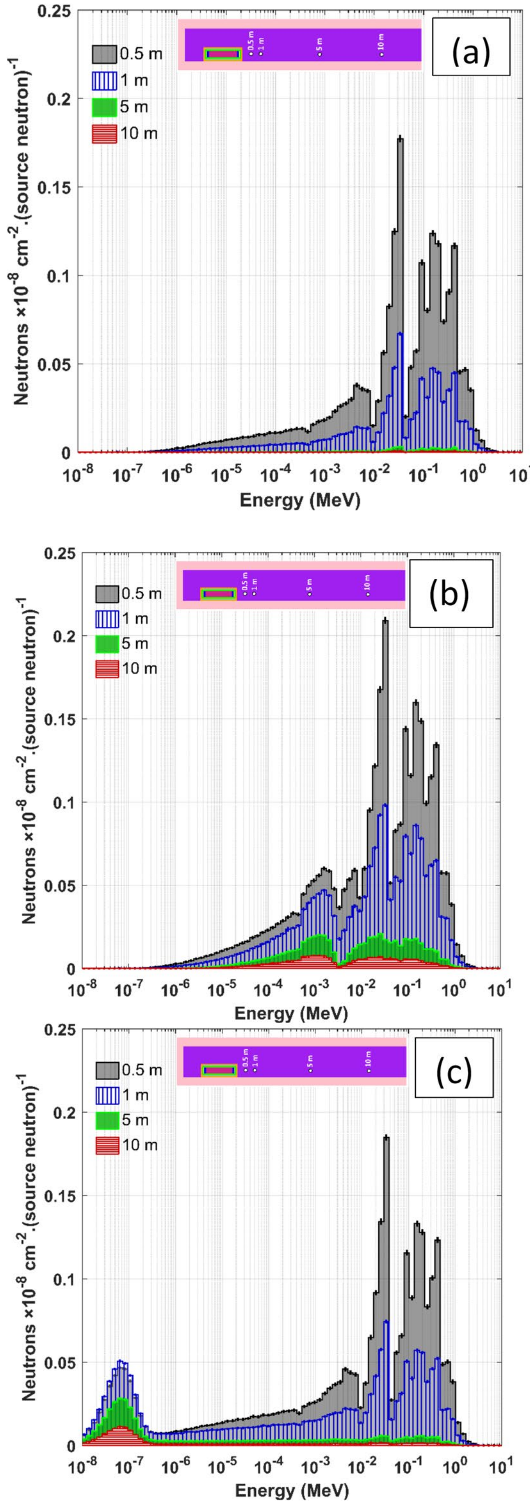

In the case of galleries with concrete walls, the neutron dose rate curve is comparatively lower by about a factor 2 (Fig. 7). The explanation for this difference lies in the neutron-moderating nuclides within the concrete. In particular, hydrogen and to some extent oxygen contribute to the thermalization of neutrons. As mentioned

Table 3 Contribution of backscattering in different host rocks

Distance (m)	Energy range (MeV)	Neutron flux at the detector [neutrons.cm^{-2}.(source neutron)$^{-1}$]		
		Free in air	**In salt gallery**	**In concrete gallery**
1.0	$<0.025\times10^{-6}$	1.17×10^{-13}	1.77×10^{-13}	6.57×10^{-10}
	0.025×10^{-6} to 1.0	7.47×10^{-9}	1.79×10^{-8}	1.53×10^{-8}
	1.0 to 10.0	8.25×10^{-11}	1.33×10^{-10}	1.11×10^{-10}
	Total	$7.56\times10^{-9}\pm0.27\%$	$1.80\times10^{-8}\pm0.20\%$	$1.60\times10^{-8}\pm0.20\%$
5.0	$<0.025\times10^{-6}$	7.03×10^{-14}	5.79×10^{-14}	3.78×10^{-10}
	0.025×10^{-6} to 1.0	4.04×10^{-10}	5.15×10^{-9}	3.85×10^{-9}
	1.0 to 10.0	4.41×10^{-12}	2.36×10^{-11}	1.36×10^{-11}
	Total	$4.08\times10^{-10}\pm0.81\%$	$5.18\times10^{-9}\pm0.23\%$	$4.24\times10^{-9}\pm0.30\%$
10.0	$<0.025\times10^{-6}$	3.09×10^{-14}	1.34×10^{-14}	1.55×10^{-10}
	0.025×10^{-6} to 1.0	9.62×10^{-11}	1.87×10^{-9}	1.34×10^{-9}
	1.0 to 10.0	1.18×10^{-12}	7.26×10^{-11}	3.97×10^{-11}
	Total	$9.74\times10^{-11}\pm1.1\%$	$1.87\times10^{-9}\pm0.50\%$	$1.49\times10^{-9}\pm0.50\%$

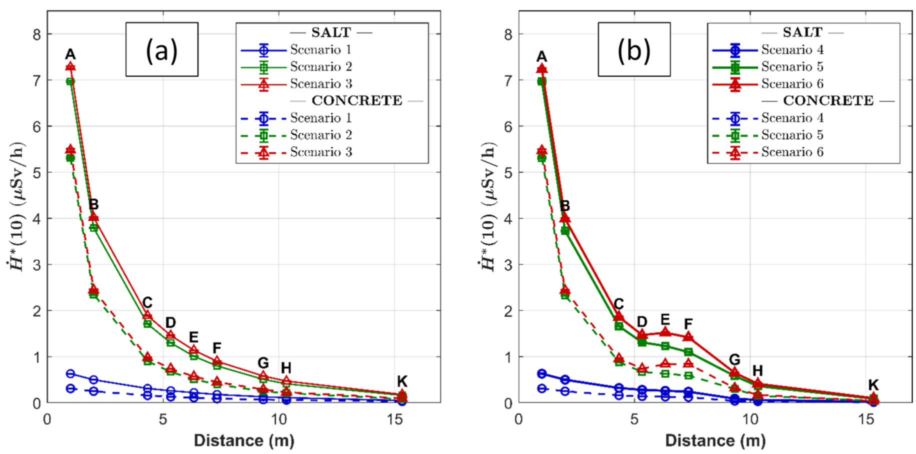

Fig. 7 Distance-dependent neutron ambient dose rate $\dot{H}^*(10)$ for the six scenarios in rock salt and with concrete walls. The figure shows scenarios with straight galleries (**a**) and with gallery branches with a right-angled geometry (**b**). The distance is specified in relation to the second cask position as described in Figs. 3b and c and 4b and c

before, the dose factor for thermal neutrons is 5, while for fast neutrons it is 20. In contrary to the concrete, these fast neutrons are the main contributor to the dose in the salt gallery.

As far as the 90° branching is concerned, one observes additional backscattering of neutrons from the walls, resulting in higher neutron dose rates in a range of approximately 20 to 60% for rock salt and 20 to 90% for concrete environments, albeit for low absolute values of about factor 2 (for concrete compared to rock salt), as mentioned above.

3.4 Results of an improved neutron scattering formalism using the DBRC method

The effects of energy- and temperature-dependent neutron scattering on the neutron dose rate were determined using MCNP® simulations for a cask placed in a straight final storage drift. For this purpose, the neutron ambient dose equivalent rates were simulated at various positions at 0.5, 1, 2, 4, 5, and 10 m distances from the cask (setup according to Figs. 2 and 3a). The calculations were performed twice using the DBRC method and comparing it to the standard MCNP® option. This was calculated for both rock salt and a concrete-lined drift. These results are shown in Fig. 8. In all cases, the dose rate is slightly lower when calculated using the DBRC method. For example, the DBRC results showed a neutron dose rate at a distance of 5 m from the cask that was 1.4% lower for rock salt and 2.7% lower for concrete lining. The statistical uncertainty of the simulation results is quite low in the range of 0.3 to 1.1%. At a distance of 5 m, it amounts to approximately 0.5%. Thus, the effect of the energy- and temperature-dependent calculations with DBRC is noticeable, albeit quite small at 300 K. The importance of using the DBRC model is thus not by the differences but rather by the range of confidence and confirmation

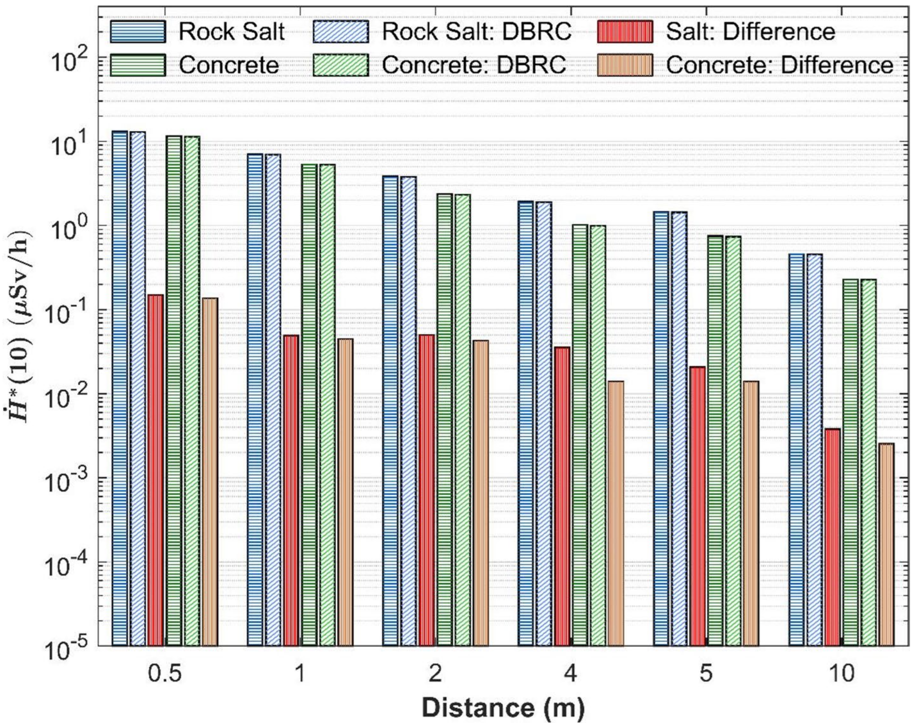

Fig. 8 Distance-dependent neutron ambient dose rate $\dot{H}^*$ (10) for the two scenarios in rock salt and with concrete walls and their respective difference. Simulation results are shown with and without the DBRC option

margins of the non-physical existing standard models in MCNP® and the feasibility to improve the scattering model within MCNP® by employing models which include relevant physical effects that were neglected before due to lack of appropriate usable models.

4 Conclusions and outlook

This study investigated aspects of scattered neutrons in the radiation field in a storage facility for high-level radioactive waste. A deep geological repository was simulated with shielding casks loaded with spent fuel rods placed inside an emplacement drift. The general-purpose Monte Carlo N-Particle code MCNP6 was employed. It has been shown that the host rock or concrete lining has a decisive influence on the radiation field and the distance-dependent neutron ambient dose rate$\dot{H}^*$ (10). The scenarios with concrete lining show a less pronounced $\dot{H}^*$ (10) compared to salt as host rock. This is due to the thermalization of a significant number of neutrons.

The general conclusion of this study is that a concrete lining results in a reduction in dose rate compared to a drift consisting only of rock salt.

The study showed a substantial influence of the numbers and geometric orientation of PET rods of the emitted neutron flux from the cask. In a salt gallery, where backscattering of neutrons significantly increases the overall radiation field, the effect of the PET rods on the backscattered neutrons is negligible compared to the corresponding scenarios in free in air.

For the investigated scenarios with right-angled geometry, it has been shown that significantly higher dose rates can occur near a gallery branch. To once again illustrate the increase in dose levels quantitatively, the measured values for detector positions E and F in scenarios 3 and 6 (see Fig. 7) are listed below for a 90° branch compared to a straight emplacement gallery. Accordingly, a 33% and 58% increase in dose, respectively, is observed at positions E and F in the salt gallery. For the corresponding scenarios in the concrete gallery, dose levels were 47% and 87% higher, respectively. Thus, an intuitive assumption that the dose is reduced behind a right-angled branch does not hold true.

As a result, the influence of backscattering must be taken into strong consideration when determining the neutron ambient dose rate $\dot{H}^*$ (10) in emplacement drifts.

The effects of energy- and temperature-dependent neutron scattering on neutron dose rate were determined using MCNP® simulations for a cask placed in straight final disposal drifts. The calculations were performed using the DBRC MCNP® option. Concerning the results for this specific study, for both the rock salt scenario and the scenario in a concrete-lined drift, the neutron ambient dose rate $\dot{H}^*$ (10) was slightly but noticeably lower in the simulations performed using the DBRC method. However, the temperature of the gallery walls was comparatively low at 300 K, so that, as known, the DBRC method has a smaller effect. The significance of this model is in that it allows us to correctly explain physical phenomena that were not previously taken into account. Strictly speaking, the simulations performed with standard methods of MCNP® so far, were actually to not correct in the relevant energy range up to 50 keV. Even if in this study the effect of the DBRC method was not so big, the impact could be different for other material inventories, i.e., in the presence of large amounts of heavy isotopes, or under adverse scenarios, i.e., in the case of a temperature rise in the spent fuel cask. This has become particularly evident in studies of neutron scattering with heavy nuclei with gas cooling, e.g. uranium isotopes [1]. It should be noted that the neutron scattering spectrum also includes energies up to the MeV range. At high energies, the influence of the DBRC correction is negligible compared to its influence in the epithermal, energy-resolved resonance range. For the future, there are plans to use a better suitable model, the well-known Blatt-Biedenharn model [3], which theoretically includes further the essential separated handling of p- and s-resonances for scattering processes for energies up to 1–2 MeV.

Acknowledgements This study was conducted as part of a Master thesis submitted to the SAfe and REliable Nuclear Applications (SARENA) program, Nuclear Reactors Operation and Safety (NROS) track.

Author contributions S.B. provided the basis for the manuscript, F.B. developed the main concept of the study and wrote the main part of the manuscript, S.B. and R.D. reviewed the manuscript, F.B. was responsible for the Monte Carlo simulations, S.B. and R.D. prepared the input data and analyzed the simulation results, S.B. created the figures.

Funding S.B. was supported by a scholarship from the SAfe and REliable Nuclear Applications (SARENA) program, Nuclear Reactors Operation and Safety (NROS) track.

Data availability The datasets used and/or analyzed during the current study are available from the corresponding author on reasonable request.

Declarations

Ethics approval and consent to participate Not applicable.

Consent to publish declaration Not applicable.

Competing interests The authors declare no competing interests.

References

1. Becker B. On the influence of the resonance scattering treatment in Monte Carlo codes on high temperature reactor characteristics. PhD thesis. University of Stuttgart; 2010.
2. Biswas S. Evaluation of Radiation Field in a High Level Waste Repository in view of Gallery Characterization and Different Scattering Kernels, Master thesis. Lappeenranta, Finland: Lappeenranta–Lahti University of Technology LUT; 2024. https://urn.fi/URN:NBN:fi-fe2024101077050.
3. Blatt JM, Biedenharn LC. 1952. The Angular Distribution of Scattering and Reaction Cross Sections, Rev. Mod. Phys. 24, 258, 1952.
4. Bollingerfehr W, Filbert W, Lerch C, Tholen M. (2011). Endlagerkonzepte. Bericht zum Arbeitspaket 5 Vorläufige Sicherheitsanalyse für den Standort Gorleben. Gesellschaft für Anlagen und Reaktorsicherheit (GRS) GmbH. ISBN: 978-3-939355-48-9. GRS-272.
5. Filbert W, Engelmann HJ, Heda M, Neydek J. 1995. Direkte Endlagerung aus-gedienter Brennelemente (DEAB) - Handhabungsversuche zur Streckenlagerung. Tech. Rep. 82. Deutsche Gesellschaft für den Bau und Betrieb von Endlagern für Abfallstoffe mbH (DBE).
6. ICRP. 1996. International Commission on Radiological Protection. Conversion Coefficients for use in Radiological Protection against External Radiation. ICRP Publication 74, Annals of the ICRP, Volume 26 (3–4), 1996.
7. ICRP. 2007. The 2007 Recommendations of the International Commission on Radiological Protection. ICRP Publication 103, Annals of the ICRP, Volume 37 (2–4), 2007.
8. Janberg K, Spilker H. Status of the Development of Final Disposal Casks and Prospects in Germany. Nucl Technol. 1998;121(2):136–47. https://doi.org/10.13182/NT98-A2826.
9. Nucleonica GH. 2024. Nucleonica Nuclear Science Portal (www.nucleonica.com), Version 3.0.661, Karlsruhe, 2024.
10. Pang B, Saurí Suárez H, Becker F. Individual dosimetry in disposal repository of heat-generating nuclear waste. Radiat Prot Dosim. 2016;170(1–4):387–92.
11. Peiffer, McStocker. Abfallspezifikation und Mengengerüst, Basis Ausstieg aus der Kernenergienutzung; Bericht zum Arbeitspaket 3 Vorläufige Sicherheitsanalyse für den Standort Gorleben. Gesellschaft für Anlagen- und Reaktorsicherheit (GRS) gGmbH; 2011. pp. GRS–278.
12. Rothenstein W, Dagan R. Ideal gas scattering kernel for energy dependent cross-sections. Ann Nucl Energy. 1998;25(4):209–22. https://doi.org/10.1016/S0306-4549(97)00063-7.
13. Saurí Suárez H, Pang B, Becker F, et al. Monte-Carlo based comparison of the personal dose for emplacement scenarios of spent nuclear fuel casks in generic deep geological repositories. ATW Atomwirtschaft-Atomtechnik. Int J Nuclear Power. 2017;62:384–8. https://publikationen.bibliothek.kit.edu/1000192580.
14. Saurí Suárez H. Individual dosimetry in disposal facilities for high-level nuclear waste. 32.01.15; LK 01. PhD thesis. Karlsruher Institut für Technologie (KIT); 2018. https://doi.org/10.5445/IR/1000084032.
15. Stahlmann J, Mintzlaff V, Leon-Vargas R. 2015. ENTRIA-Arbeitsbericht-03: Generische Tiefenlagermodelle mit Option zur Rückholung der radioaktiven Reststoffe: Geologische und Geotechnische Aspekte für die Auslegung. ISSN (Print): 2367–3532, ISSN (Online): 2367–3540, Technische Universität Braunschweig, Braunschweig, Germany, in German. https://www.irs.uni-hannover.de/fileadmin/irs/entria/Dokumente/Arbeitsberichte/ENTRIA-Arbeitsbericht-03_Stahlmann_GenerischeTiefenlagermodelle.pdf (in German, Access date: 22 Apr 2026).
16. Werner CJ, Armstrong JC, Brown FB, Bull JS, Casswell L, Cox LJ, Dixon DA, Forster RA, Goorley JT, Hughes HG, Favorite JA, Martz RL, Mashnik SG, Rising ME, Solomon CJ Jr., Sood A, Sweezy JE, Zukaitis AJ, Anderson CA, Elson JS, Johns D Jr., McKinney RC, McMath GW, Hendricks GE, Pelowitz JS, Prael DB, Booth RE, James TE, Fensin MR, Wilcox ML, Kiedrowski TA. B. C., 2017. MCNP User's Manual Code Version 6.2. Los Alamos National Laboratory Tech. Rep. LA-UR-17-29981. Los Alamos, NM, USA. October 2017.
17. Wilson WB, Perry RT, Charlton WS, Parish TA. 2009. Sources: A code for calculating (alpha, n), spontaneous fission, and delayed neutron sources and spectra, Progress in Nuclear Energy, 51, Issues 4–5, Pages 608–13, ISSN 0149–1970. https://doi.org/10.1016/j.pnucene.2008.11.007

Authors and Affiliations

Sushanta Biswas[1,2] · Frank B. E. Becker[1] · Ron Dagan[1]

✉ Frank B. E. Becker
frank.becker@kit.edu

1 Institute for Nuclear Waste Disposal (INE), Karlsruhe Institute of Technology (KIT), Hermann-von-Helmholtz-Platz 1, 76344 Eggenstein-Leopoldshafen, Germany

2 Institute of Nuclear Technology and Energy Systems (IKE), University of Stuttgart, Pfaffenwaldring 31, 70569 Stuttgart, Germany